Journal of The Electrochemical Society, **165** (7) A1455-A1459 (2018)
0013-4651/2018/165(7)/A1455/5/$37.00 © The Electrochemical Society

Porous SnSbNPs@3D-C Anode with Improved Stability for Sodium-Ion Battery

Wenhui Wang,[1] Liang Shi,[1,2,z] and Quan Li[1,z]

[1]*Department of Physics, The Chinese University of Hong Kong, Shatin, New Territory, Hong Kong*
[2]*Department of Chemistry, University of Science and Technology of China, Hefei 230026, People's Republic of China*

Nano-sized SnSb particles encapsulated in porous 3D carbon matrix (SnSbNPs@3D-C) is fabricated by a freeze-drying assisted method. Such a sample shows a stable cycling stability (i.e. retaining 96.5% of its first de-sodiation capacity after 100 cycles at 100mA/g) and a good rate capability (i.e. retaining 86.2% of the de-sodiation capacity when the current density increases from 100mA/g to 1A/g). We show experimental evidence that the architecture of nano-sized SnSb residing in porous structure constructed by 3D carbon effectively suppresses the particle pulverization and crack generation in the electrode upon repeated cycling, contributing to the improved electrochemical property.
 [DOI: 10.1149/2.0811807jes]

Manuscript submitted January 19, 2018; revised manuscript received April 23, 2018. Published May 11, 2018.

Practical application of sodium-ion battery (SIB) is largely limited by the available anodes with high capacity and long cycle-life.[1,2] Anodes made of Group IV and V elements have been considered as promising candidates for their high theoretical capacities with alloying/de-alloying as the storage mechanism.[3–8] Among them, the environmental friendly and cost-effective Sn appears to be one of the most promising candidates with a low average operating voltage (∼0.25V vs. Na/Na^+), which is beneficial for obtaining high energy density in a full-cell configuration.[9]

However, practical application of Sn anode is hindered by the severe capacity fading, mainly due to problems resulted from a huge volume change (∼524%, final volume versus initial volume) and drastic structural changes (i.e., $Sn \rightarrow Na_xSn$ ($x < 1$) $\rightarrow NaSn \rightarrow Na_9Sn_4 \rightarrow Na_{15}Sn_4$) upon sodiation/de-sodiation process. Forming SnSb alloy by introducing Sb has been proposed as an effective approach to improve the cycle stability as the sodiation/de-sodiation process of Sn and Sb occurs at different potential. The alloy structure then provides a buffer matrix for both Sn and Sb, i.e., the inactive Sn at specific potentials can act as conductive buffer matrix for Sb that undergoes sodiation, and vice versa,[10–17] so that the electrode integrity is maintained. This indeed helps to improve the cyclability, for example, SnSb/C (30wt%) nanocomposites can retain ∼435mAh/g after 50 cycles at 100mA/g (represents a capacity retention of 80%), while Sn/C (30wt%) nanocomposites show a fast decay to <100mAh/g within 20 cycles when processed at similar conditions.[10] However, the capacity decay persists as the large volume changes upon alloying/de-alloying remains, and the pulverization of the active materials leads to crack generation in the electrode.[10,13] To tackle this problem, several approaches have been proposed. The first approach involves creating porous structure to accommodate the volume changes. For example, Liu's group[12] synthesized SnSb-porous carbon nanofibers via electrospun, which delivers a reversible capacity of ∼340mAh/(g composite) over 200 cycles at 100mA/g. The second approach aims to reduce the size to alleviate the strain from volume change. In this approach, Kovalenko's group proposed to use monodispersed SnSb nanocrystals prepared via hot injection method[16] or chemical reduction in organic solvent,[17] the resulted colloidal SnSb alloy nanoparticles (<20nm) can maintain a reversible capacity of ∼450mAh/g over 100 cycles at 200mA/g.

In this work, we employed a facile freeze-drying assisted solid-state method to synthesize nano-sized SnSb particles encapsulated in a 3D carbon matrix (porous SnSbNPs@3D-C) as anode for SIB. The porous SnSbNPs@3D-C electrode demonstrates good cycle stability (retaining 96.5% of its first de-sodiation capacity after 100 cycles at 100mA/g) and excellent rate capability (i.e. retains 86.2% of the de-sodiation capacity, when the current density increases from 100mA/g to 1A/g). A few material factors contribute to the improved electrochemical property of such electrode. Firstly, the nano-sized SnSb particles can better withstand the stress and limit crack generation in the particles (i.e. particle pulverization).[18] Secondly, the porous structure constructed by 3D carbon can help to accommodate the volume expansion upon sodiation process, thus preventing the crack generation of the electrode. Lastly, both nano-sized (shorter Na^+ diffusion length) and porous structure (better electrolyte permeation) help to promote the rate capability of the electrode as comparing to bulk (solid, micro-sized) SnSb/C electrode.

Experimental

Synthesis of electrode materials.—All chemical reagents used in this study are analytical grade without any further purification. In a typical procedure, 0.5g polyvinyl pyrrolidone (PVP, with average molecular weight of 40000) was firstly dissolved in 50 mL deionized water. Then, 2.5g citric acid, 0.68g (3mmol) $SnCl_2 \cdot 2H_2O$, 1.002g (1.5mmol) potassium antimonyl tartrate trihydrate ($C_8H_6K_2O_{13}Sb_2 \cdot 3H_2O$), and 15g KCl were added into the above solution. After stirring for 10 min, the as-obtained transparent solution was rapidly frozen by pouring into liquid nitrogen at a constant speed. Subsequently, the water in the mixture was removed by freeze-drying process and the obtained sponge-like sample was ground into powder. Then, the composite powder was subjected to annealing at 700°C for 2h with a ramp rate of 3°C/min under H_2/Ar (with 10vol% H_2) mixture flow. At last, the as-synthesized products were washed by deionized water for several times to remove the KCl template, and SnSbNPs@3D-C was obtained.

Two control samples (i.e. SnSb/C and 3D-C) were also prepared using the same freeze-drying assisted method. However, for SnSb/C, no PVP and citric acid were used; for 3D-C (Figure S1), no $SnCl_2 \cdot 2H_2O$ and $C_8H_6K_2O_{13}Sb_2 \cdot 3H_2O$ were used.

Material characterizations.—The overall crystallinity and the general morphology of the product was examined by X-ray diffraction (XRD, SmartLab, Rigaku) with Cu Kα radiation ($\lambda = 0.1541$ nm) and field emission scanning electron microscopy (FESEM, Quanta 200, FEI) under acceleration voltage of 20kV, respectively. The XRD patterns of as-prepared samples and the electrodes were collected with a scan rate of 8°/min under 40kV and 40mA, and a scan rate of 0.2°/min under 40kV and 80mA, respectively. To avoid any possible exposure to air, the electrodes were sealed with 2 mil Kapton tape in argon-filled glove box before XRD experiments. The carbon content of the product was estimated via thermogravimetric analysis (TGA) in a temperature range of 50–700°C with a ramping rate of 10°C/min under oxygen flow. N_2 adsorption and desorption isotherms (ADI) were collected by the ASAP 2000 after the sample was vacuum dried at 120°C for 6h. Raman spectra were collected using a Micro Raman spectrometer

[z]E-mail: sliang@ustc.edu.cn; liquan@phy.cuhk.edu.hk

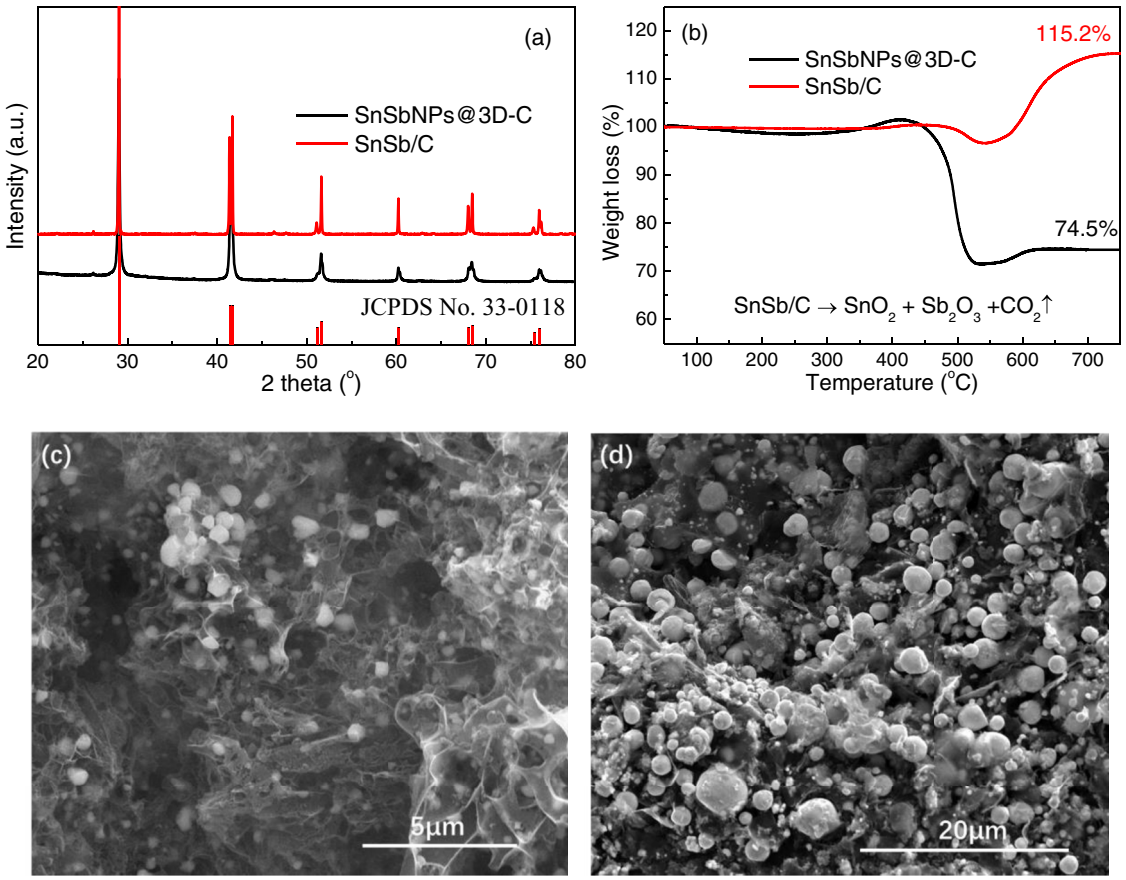

Figure 1. (a) XRD patterns and (b) thermogravimetric curves of the as-prepared SnSbNPs@3D-C and SnSb/C; SEM images of (c) SnSbNPs@3D-C and (d) SnSb/C. 74.5% and 115.2% in (b) indicates the weight percentage of the corresponding final products of SnSbNPs@3D-C and SnSb/C, respectively.

(RM-1000, Renishaw Co., Ltd.) with a 10mW helium neon laser at 514 nm.

Electrochemical measurements.—The anode electrodes were prepared by mixing active material with multi-wall carbon nanotubes (MWCNT) conductive additives and sodium carboxymethyl cellulose (NaCMC) binder with a mass ratio of 80:10:10 in water to form homogeneous slurry. The slurry was then coated on Cu foil followed by a vacuum drying at 60°C overnight. Electrodes with diameter of 16mm and active material loading of ∼1.0mg/cm^2 were then cut out from the dried coating.

The electrodes were assembled into CR2032 coin-type cells with Na foil and glass fiber filter (GD-120) as reference electrode and separator, respectively. 1M $NaClO_4$ in a mixture of propylene carbonate and fluoroethylene carbonate (PC/FEC, 95:5, by volume) was used as the electrolyte.

The Na-ion cells were galvanostatically charged/discharged using multichannel battery test system (Neware, Shenzhen). 10 minutes of rest was employed between each charge and discharge process. Cyclic voltammetry was carried out via electrochemical workstation (CHI 760E, Shanghai Chenhua Instrument Co., Ltd.) at a scanning rate of 50uV/s. Electrochemical impedance spectroscopy (EIS) was carried out via electrochemical workstation (CHI 760E) with a AC signal of 10mV.

All experiments were carried out at room temperature (24 ± 2°C) unless specified otherwise.

Results and Discussion

Material characterizations.—To validate the importance of 3D carbon structure in SnSbNPs@3D-C, a control sample without 3D carbon matrix, SnSb/C, is also presented in this work. Synthesis of the two samples can be found in the Experimental section. Figure 1a shows the XRD patterns of the as-prepared SnSbNPs@3D-C and SnSb/C samples. The peaks in both XRD data can be indexed to hexagonal SnSb with space group of R-3m (166) (JCPDS No. 33-0118). TGA was used to estimate the carbon contents in the sample (Figure 1b). The net weight change in the samples is the difference of loss from carbon combustion and gain from SnSb oxidation. Consequently, the carbon in SnSbNPs@3D-C and SnSb/C are estimated to be ∼39.6wt% and ∼6.6wt%, respectively. It should be noted that the residue carbon in SnSb/C is originated from the thermal decomposition of antimony source (i.e. $C_8H_6K_2O_{13}Sb_2{\cdot}3H_2O$) during preparation.

SEM image of the SnSbNPs@3D-C sample (Figure 1c and Figure S2) shows that SnSb nanoparticles with sizes ranging from tens to hundreds of nanometers are encapsulated in the porous carbon network, which is expected to serve as effective buffer to accommodate the volume changes of SnSb upon sodiation/de-sodiation process. As a comparison, the size of SnSb particles in the SnSb/C sample (Figure 1d) is in the range of micrometers. It also appears denser than the SnSbNPs@3D-C sample. Using N_2 ADI (Figure S3), the Brunauer-Emmett-Teller (BET) surface areas of SnSbNPs@3D-C and SnSb/C samples are estimated as 135.4m^2/g and 68.7m^2/g, respectively. This BET difference is consistent with the SEM observations.

Electrochemical characterizations.—Figure 2a shows the cyclic voltammograms (CVs) of SnSbNPs@3D-C electrode collected at a scanning rate of 50uV/s. During the first cathodic scan, the reduction peaks between 0.8V and 1.2V originate from modification of the solid-electrolyte interphase (SEI),[12,19] which are absent in subsequent cycles. The strong reduction peak at ∼0.4V is ascribed to initial sodiation of SnSb to form Na_3Sb and Sn; while the latter two at 0.2V

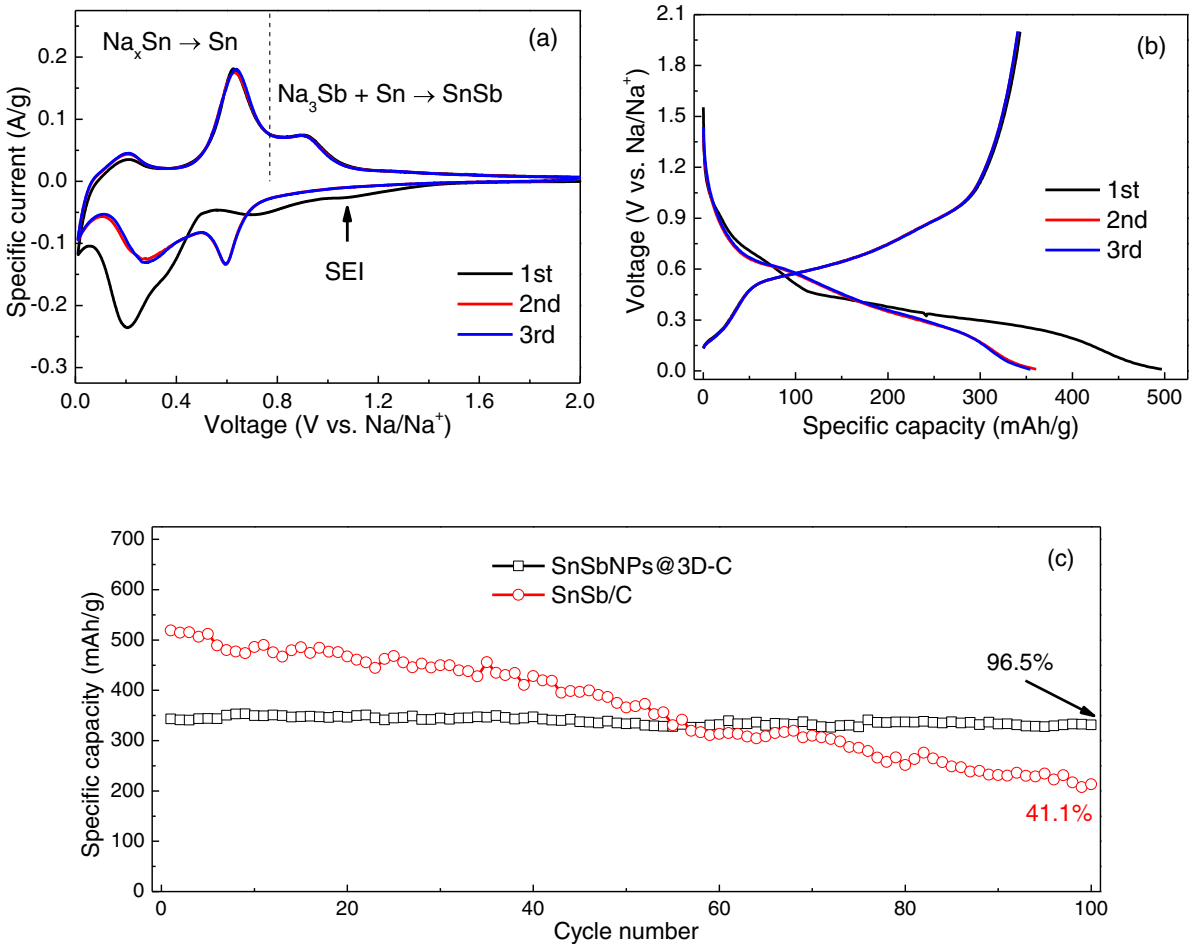

Figure 2. (a) Cyclic voltammogram of SnSbNPs@3D-C electrode at a scan rate of 50uV/s, (b) charge/discharge curves of SnSbNPs@3D-C electrode at current density of 100mAh/g, and (c) comparison of cycle performance of SnSbNPs@3D-C electrode and SnSb/C electrode at 100mA/g.

and ~0V are due to further sodiation of Sn to form Na_xSn.[10,12,14] In subsequent cathodic scans, the reduction peaks of ~0.4V and ~0.2V shift to ~0.6V and ~0.3V, respectively, after the electrode material being activated in the first scan. In the anodic scans, three oxidation peaks at ~0.2V, ~0.6V, and ~0.9V can be observed. The first two peaks can be ascribed to the de-sodiation of Na-Sn alloys; while the third one originates from the de-sodiation of Na_3Sb and the reformation of SnSb alloys.[10,12,14] The CV curves show consistent features except for the first cathodic scan, indicating the sodiation/de-sodiation process is reversible after the initial activation. These electrochemical features are consistent with the sodiation/de-sodiation voltage profiles (Figure 2b) tested at 100mA/g. Similar CV characteristics and voltage profiles are observed in the SnSb/C sample (Figure S5), suggesting similar electrochemistry in the two samples.

Figure 2c displays the capacity changes of SnSbNPs@3D-C electrode and SnSb/C electrode when cycled in 2.0–0.01V at 100mA/g. The porous SnSbNPs@3D-C electrode delivers a first de-sodiation capacity of ~344mAh/g, and 96.5% of it has been retained (i.e. ~332mAh/g) after 100 cycles. As a comparison, the SnSb/C electrode only delivers a de-sodiation capacity of ~213mAh/g at 100th cycle, despite of its higher initial de-sodiation capacity (i.e. ~519mAh/g). The higher initial de-sodiation capacity of SnSb/C, as compared to that of SnSbNPs@3D-C, is mainly due to the reduced carbon content in the sample, as the Na storage capability of C is much lower than that of SnSb (Figure S6). In addition, both samples can reach high Coulombic efficiency of ~98.3 upon extended cycles (Figure S7), and these results are comparable to previous reports on SnSb.[10–13,15–17]

Figure 3 shows the typical voltage profiles of SnSbNPs@3D-C electrode and SnSb/C electrode at different current densities. The porous SnSbNPs@3D-C electrode shows only slight increase of polarization (i.e. a slightly larger voltage gap between sodiation/de-sodiation process) as the charge/discharge current density increases from 100mA/g to 1A/g, while in the case of SnSb/C electrode, a large increase of polarization occurs especially when the current density is higher than 500mA/g. A much better rate capability of SnSbNPs@3D-C electrode is obtained as compared to the SnSb/C electrode. Consistent results on the rate capacity retention are obtained in the two samples (Figure S8). For example, when charging/discharging at 1A/g, porous SnSbNPs@3D-C electrode retains 86.2% of its capacity at 100mA/g, while the SnSb/C electrode only keeps 60.8% of its capacity obtained at 100mA/g. The improved rate capability of SnSbNPs@3D-C electrode should be resulted from the unique 3D porous structure consisted by carbon and nano-sized SnSb grains, both of which facilitate faster Na^+ diffusion.

Post-analysis after electrochemical cycling.—To understand the cycle stability of both electrodes, SEM images and XRD were collected at specific stages of samples (i.e. fresh electrode without subjecting to electrochemical test, electrode being sodiated to 10mV, and electrode being de-sodiated to 2.0V after 100 cycles).

The as-fabricated porous SnSbNPs@3D-C electrode (Figure 4a) shows porous structure, and SnSb particles of several hundred nanometers can be seen. After being sodiated to 10mV (Figure 4b), the integrity of the electrode is well-maintained and cracks can be observed on neither the electrode nor the individual SnSb particle. Even after 100 cycles, the integrity of the electrode is well-maintained without obvious crack formation. These results are consistent with the stable cycling stability shown in Figure 2c.

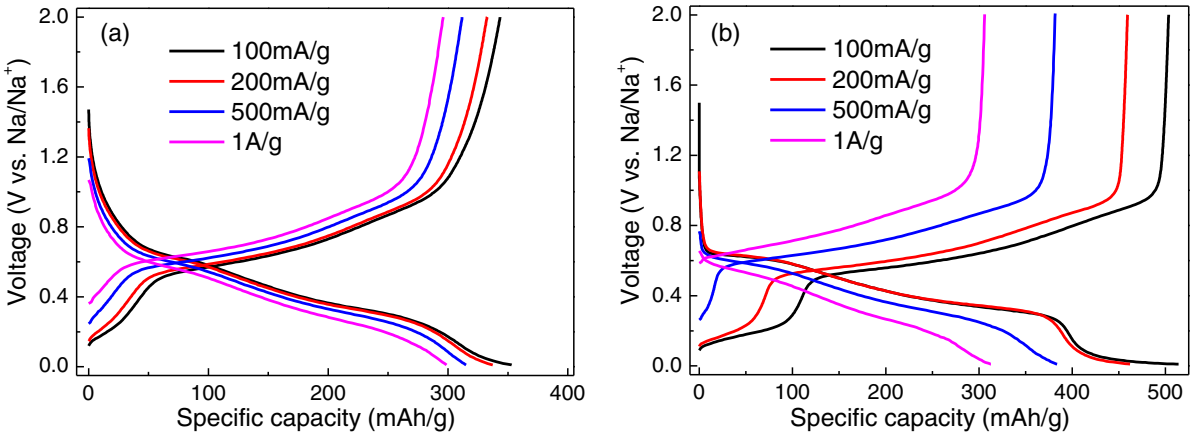

Figure 3. Typical charge/discharge curves of (a) SnSbNPs@3D-C electrode and (b) SnSb/C electrode at different current densities.

As a comparison, the as-fabricated SnSb/C electrode (Figure 4d) shows a relatively dense structure. After being sodiated to 10mV, the electrode lost its integrity as large cracks are visible. In addition, individual SnSb particles are also found to pulverize after sodiation (inset of Figure 4e). After 100 cycles, many cracks can be found throughout the sample. The particle pulverization and crack generation in SnSb/C electrode revealed by the SEM images provide an explanation for its relatively fast capacity fading (Figure 2c).

The evolution of electrode integrity revealed by the SEM images is consistent with the results of EIS shown in Figure S10. Comparing to SnSb/C electrode, SnSbNPs@3D-C electrode shows much smaller ohmic resistance (i.e., much better electronic contact among active materials, as well as between electrode laminate and current collector) after the first cycle, and also less increase in charge transfer resistance upon extended cycles.

The ex-situ XRD (Figure S6) shows that the reformation of SnSb is achieved after de-sodiation process for SnSbNPs@3D-C electrode over 100 cycles; while little signal of SnSb is observed for SnSb/C electrode only after 1 cycle, indicating either its low crystallinity or the failure of SnSb reformation at the end of de-sodiation process in such a sample.

To summary the above finding, a few factors contribute the good cycle stability of SnSbNPs@3D-C. Firstly, the small size of SnSb in SnSbNPs@3D-C releases the stress, making it survive without cracking upon repeated cycling. Secondly, the 3D carbon with open structure not only provides space for volume changes, but also help to accommodate the stress itself, thus preventing the electrode pulverization (i.e., loss of contact within electrode). Finally, the physi-chemi microenvironment in the sample (3D vs. no-3D) also determines the local chemistry and thus the re-formation of crystalline SnSb or not, may also contributes to the improve the stability.

Conclusions

A facile freeze-drying assisted solid-state route is proposed to synthesize SnSb particles with sizes ranging from tens to hundreds of nanometers encapsulated in porous 3D carbon matrix. The small size of SnSb and the porous structure formed by 3D carbon matrix in

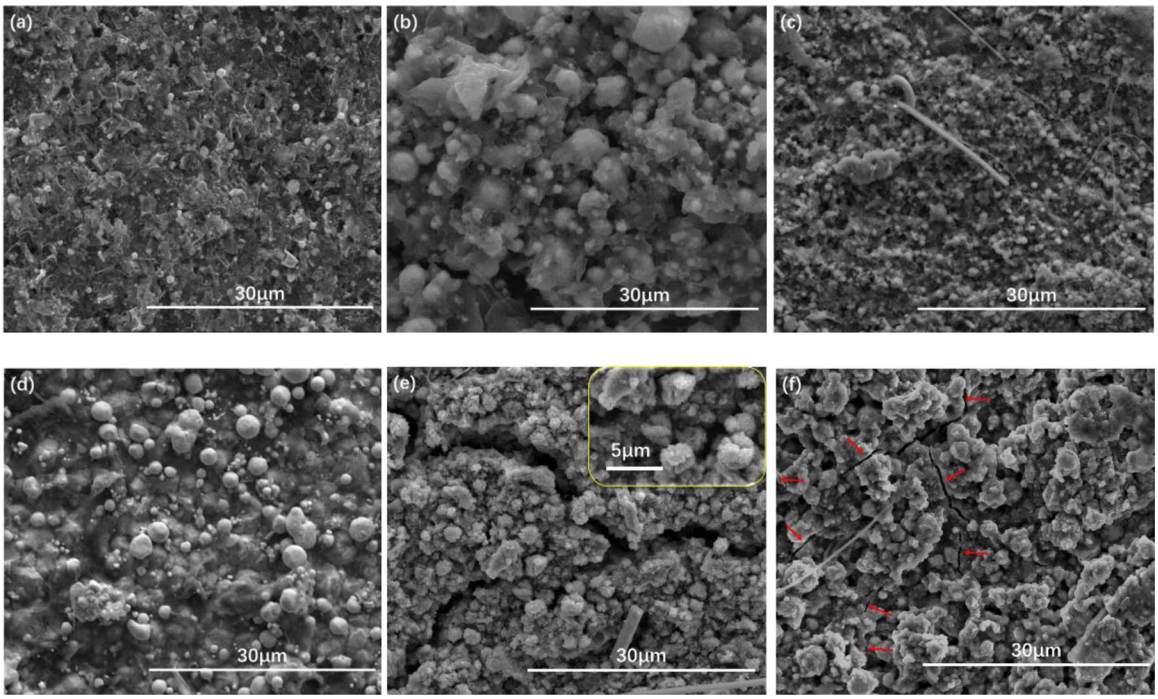

Figure 4. SEM images of (a-c) SnSbNPs@3D-C electrode and (d-f) SnSb/C electrode. (a, c) Pristine, (b, e) after being sodiated to 10mV at 100mA/g, and (c, f) after 100 cycles at 100mA/g.

SnSbNPs@3D-C electrode make it more resistant to SnSb particle pulverization and crack generation of the whole electrode upon repeated electrochemical cycling. As a result, SnSbNPs@3D-C electrode delivers a reversible capacity of ∼332mAh/g with a capacity retention of ∼96.5% over 100 cycles at 100mA/g. When charging/discharging at 1A/g, the electrode maintains a de-sodiation capacity of ∼299mAh/g, retaining 86.2% of the de-sodiation capacity at 100mA/g.

Acknowledgments

This work is supported by RGC/GRF under project No. 14316716.

ORCID

Wenhui Wang https://orcid.org/0000-0002-2449-619X
Liang Shi https://orcid.org/0000-0002-2397-0291

References

1. M. Lao, Y. Zhang, W. Luo, Q. Yan, W. Sun, and S. X. Dou, *Advanced materials*, (2017).
2. W. Wang, J. Zhang, D. Y. W. Yu, and Q. Li, *Journal of Power Sources*, **364**, 420 (2017).
3. L. D. Ellis, T. D. Hatchard, and M. N. Obrovac, *Journal of the Electrochemical Society*, **159**, A1801 (2012).
4. S. Komaba, Y. Matsuura, T. Ishikawa, N. Yabuuchi, W. Murata, and S. Kuze, *Electrochemistry Communications*, **21**, 65 (2012).
5. J. Qian, Y. Chen, L. Wu, Y. Cao, X. Ai, and H. Yang, *Chemical communications*, **48**, 7070 (2012).
6. A. Darwiche, C. Marino, M. T. Sougrati, B. Fraisse, L. Stievano, and L. Monconduit, *Journal of the American Chemical Society*, **134**, 20805 (2012).
7. L. D. Ellis, B. N. Wilkes, T. D. Hatchard, and M. N. Obrovac, *Journal of the Electrochemical Society*, **161**, A416 (2014).
8. J. Qian, X. Wu, Y. Cao, X. Ai, and H. Yang, *Angew Chem Int Ed Engl*, **52**, 4633 (2013).
9. N. Yabuuchi, K. Kubota, M. Dahbi, and S. Komaba, *Chem Rev*, **114**, 11636 (2014).
10. L. Xiao, Y. Cao, J. Xiao, W. Wang, L. Kovarik, Z. Nie, and J. Liu, *Chemical communications*, **48**, 3321 (2012).
11. A. Darwiche, M. T. Sougrati, B. Fraisse, L. Stievano, and L. Monconduit, *Electrochemistry Communications*, **32**, 18 (2013).
12. L. Ji, M. Gu, Y. Shao, X. Li, M. H. Engelhard, B. W. Arey, W. Wang, Z. Nie, J. Xiao, C. Wang, J. G. Zhang, and J. Liu, *Advanced materials*, **26**, 2901 (2014).
13. J.-C. Kim and D.-W. Kim, *Electrochemistry Communications*, **46**, 124 (2014).
14. L. Baggetto, H.-Y. Hah, J.-C. Jumas, C. E. Johnson, J. A. Johnson, J. K. Keum, C. A. Bridges, and G. M. Veith, *Journal of Power Sources*, **267**, 329 (2014).
15. I. T. Kim, S.-O. Kim, and A. Manthiram, *Journal of Power Sources*, **269**, 848 (2014).
16. M. He, M. Walter, K. V. Kravchyk, R. Erni, R. Widmer, and M. V. Kovalenko, *Nanoscale*, **7**, 455 (2015).
17. M. Walter, S. Doswald, and M. V. Kovalenko, *J. Mater. Chem. A*, **4**, 7053 (2016).
18. F. Luo, B. Liu, J. Zheng, G. Chu, K. Zhong, H. Li, X. Huang, and L. Chen, *Journal of The Electrochemical Society*, **162**, A2509 (2015).
19. S. Komaba, T. Ishikawa, N. Yabuuchi, W. Murata, A. Ito, and Y. Ohsawa, *ACS applied materials & interfaces*, **3**, 4165 (2011).